Nonequilibrium Phase Transition in a Dilute Rydberg Ensemble

C. Carr, R. Ritter, C. G. Wade, C. S. Adams, and K. J. Weatherill

Department of Physics, Joint Quantum Centre (JQC) Durham-Newcastle, Durham University,
South Road, Durham DH1 3LE, United Kingdom
(Received 28 March 2013; published 10 September 2013)

We demonstrate a nonequilibrium phase transition in a dilute thermal atomic gas. The phase transition, between states of low and high Rydberg occupancy, is induced by resonant dipole-dipole interactions between Rydberg atoms. The gas can be considered as dilute as the atoms are separated by distances much greater than the wavelength of the optical transitions used to excite them. In the frequency domain, we observe a mean-field shift of the Rydberg state which results in intrinsic optical bistability above a critical Rydberg number density. In the time domain, we observe critical slowing down where the recovery time to system perturbations diverges with critical exponent $\alpha = -0.53 \pm 0.10$. The atomic emission spectrum of the phase with high Rydberg occupancy provides evidence for a superradiant cascade.

Nonequilibrium systems displaying phase transitions are found throughout nature and society, for example, in ecosystems, financial markets, and climate [1]. The steady state of a nonequilibrium system is a dynamical equilibrium between driving and dissipative processes. In atomic physics, one of the most studied nonequilibrium phase transitions is optical bistability, where the driving is provided by a resonant laser field and the dissipation is inherent in the atom-light interaction. In most examples of optical bistability, feedback is provided by an optical cavity, as in the pioneering work of Gibbs [2,3]. However, bistability can also arise in systems where many dipoles are located within a volume which is much smaller than the optical wavelength; in this case, the feedback is due to resonant dipole-dipole interactions [4,5]. This latter case is known as intrinsic optical bistability [6] and has, so far, only been observed in an up-conversion process between densely packed Yb^{3+} ions in a solid-state crystal host cooled to cryogenic temperatures [7]. Intrinsic optical bistability generally cannot be observed for simple two-level systems such as atomic gases, because the resonance broadening, which is larger than the line shift [8], suppresses the bistable response [9,10].

A solution to this problem is provided by highly excited Rydberg states, where the dipole-dipole induced level shifts between neighboring states can be much larger than the excitation linewidth. This property of optical excitation of Rydberg atoms known as dipole blockade [11] enables a diverse range of applications in quantum many-body physics, quantum information processing [12], nonlinear optics [13], and quantum optics [14–17]. An interesting feature of Rydberg systems is that the range of the interaction can be much larger than the optical excitation wavelength, giving rise to nonlocal interactions [18]. This also creates the possibility of observing intrinsic optical bistability, and hence, nonequilibrium phase transitions [19] over macroscopic, optically resolvable length scales.

In this Letter, we demonstrate a nonequilibrium phase transition in a thermal Rydberg ensemble. In contrast to previous experiments, we directly observe optical bistability in the transmission of the probe light without the requirement for cryogenics [7] or cavity feedback [2]. We distinguish between the phases of low and high Rydberg occupancy using fluorescence spectroscopy and confirm the first-order phase transition through the observation of a critical slowing down in the temporal response of the ensemble. Our observation of a nonequilibrium phase transition in a dilute atomic system provides a new platform to study the transition between classical mean-field and microscopic quantum dynamics [20,21].

To illustrate the origin of the nonequilibrium phase transition in our system, we begin by considering the
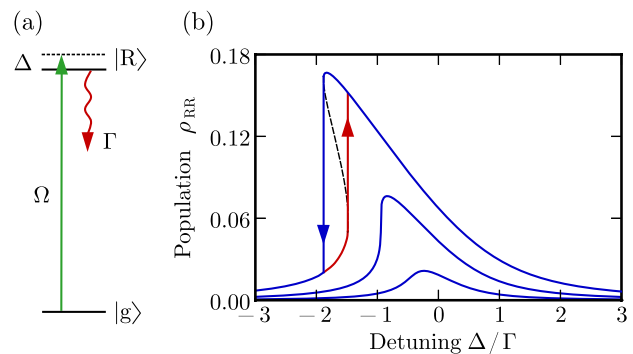

FIG. 1 (color online). Theoretical model for the cooperative optical response of the ensemble. (a) Simplified two-level model with ground state $|g\rangle$ and Rydberg state $|R\rangle$. The levels are coupled by a laser with Rabi frequency Ω and detuning from resonance Δ. (b) Rydberg state population ρ_{RR} as a function of laser detuning Δ for increasing Rabi frequency Ω. As a result of the cooperative excitation-dependent shift, the response exhibits intrinsic optical bistability with hysteresis dependent upon the history of the ensemble. Theoretical parameters: interaction strength $V/\Gamma = -11$ and Rabi frequency $\Omega/\Gamma = (0.15, 0.3, 0.5)$.

simple two-level atom shown in Fig. 1(a) with ground state $|g\rangle$ and Rydberg state $|R\rangle$. The levels are coupled by a laser with Rabi frequency Ω and detuning from resonance Δ. Using standard semiclassical analysis, the time evolution of the system can be described using the Lindblad master equation for the single-particle density matrix. To include the effect of dipole-dipole interactions between atoms in state $|R\rangle$, we use a classical approximation to the many-body quantum dynamics [20] and introduce a mean-field shift of the Rydberg state, proportional to its steady-state population. Coherent dynamics has been observed in thermal ensembles by operating on ultrashort time scales, where the Rydberg interactions appear as a dephasing of the Rabi oscillations due to the broad distribution of inter-atomic distances [22]. However, over longer time scales or in steady state as in our experiment, the interactions between Rydberg atoms result in a mean-field shift. In this limit, the laser detuning $\Delta \to \Delta - V\rho_{RR}$ where V is the dipole-dipole interaction term and ρ_{RR} is the population of the Rydberg state. The interaction term V corresponds to the sum of the dipole-dipole interaction over the excitation volume [23].

The optical Bloch equations for the two-level system can be written as
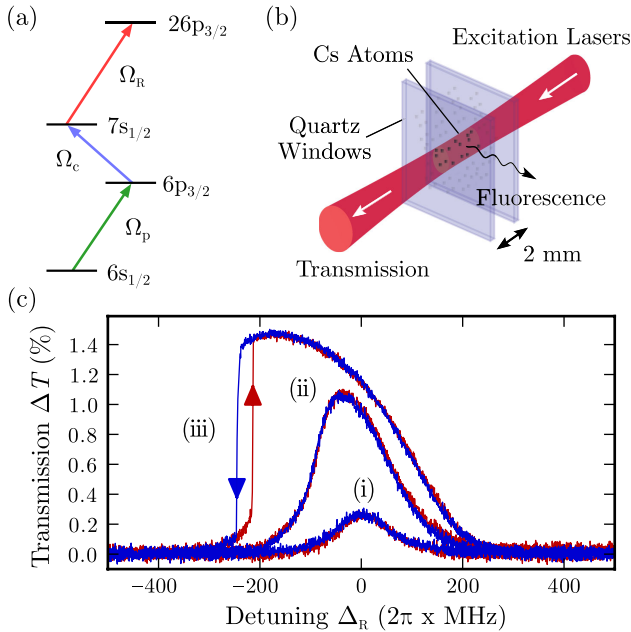

(a)

(b)

(c)

FIG. 2 (color online). (a) Three-photon excitation scheme to Rydberg states in cesium. (b) Schematic of the experimental setup. The three excitation lasers copropagate through a 2 mm vapor cell. The nonequilibrium dynamics is probed by measuring the transmission of the probe laser or analyzing the emitted fluorescence. (c) Experimental optical response ΔT as a function of Rydberg laser detuning Δ_R for Rydberg Rabi frequency Ω_R increasing from (i) to (iii). Experimental parameters: ground-state density $\mathcal{N} = 4.3 \times 10^{12}$ cm^{-3}, probe Rabi frequency $\Omega_p = 2\pi \times 37$ MHz, coupling Rabi frequency $\Omega_c = 2\pi \times 77$ MHz, and Rydberg Rabi frequency $\Omega_R = 2\pi \times (14, 36, 74)$ MHz.

$$\dot{\rho}_{gR} = i\Omega\left(\rho_{RR} - \frac{1}{2}\right) + i(\Delta - V\rho_{RR})\rho_{gR} - \frac{\Gamma}{2}\rho_{gR}, \quad (1a)$$

$$\dot{\rho}_{RR} = -\Omega \text{Im}(\rho_{gR}) - \Gamma\rho_{RR}, \quad (1b)$$

where the off-diagonal coherence terms $\rho_{Rg} = \rho_{gR}^*$ and the diagonal population terms $\rho_{gg} = 1 - \rho_{RR}$. The steady-state solution for the Rydberg population ρ_{RR} as a function of laser detuning Δ is shown in Fig. 1(b) for increasing Rabi frequency Ω. As the cooperative shift is dependent on the Rydberg population, the line shape becomes asymmetrical and eventually exhibits bistability with hysteresis dependent on the direction in which the detuning is varied (shown by the arrows). In the bistable region, there is also an unstable state (shown by the dashed curve) which cannot be measured experimentally. At the critical transition, there is an abrupt change in the atomic dynamics. The solution of Eq. (1) can be found in the Supplemental Material [24].

To experimentally observe a nonequilibrium phase transition in a dilute medium, we use a resonant multi-photon excitation scheme in a thermal Cs vapor, as shown in Fig. 2(a) [25]. In the simple theoretical analysis above Doppler averaging is not considered; however, by using a multiphoton scheme, we excite only a narrow velocity distribution of atoms [26] and can therefore access a regime where the mean-field shift between Rydberg states far exceeds the Doppler width of the excitation. The optical Bloch model for the multiphoton scheme is presented in the Supplemental Material [27]. A schematic of the experimental setup is shown in Fig. 2(b). A thermal vapor of Cs atoms is confined in a quartz cell with an optical path length of 2 mm. The atoms are driven into the $26p_{3/2}$ Rydberg state using three excitation lasers which copropagate through the cell. The probe laser, with wavelength $\lambda_p = 852.3$ nm, Rabi frequency Ω_p, and waist $w_p = 150$ μm is frequency stabilized to the $|6s_{1/2}, F = 4\rangle \to |6p_{3/2}, F' = 5\rangle$ transition. The coupling laser, with wavelength $\lambda_c = 1469.9$ nm, Rabi frequency Ω_c, and waist $w_c = 80$ μm is stabilized to the $|6p_{3/2}, F' = 5\rangle \to |7s_{1/2}, F'' = 4\rangle$ transition using excited-state polarization spectroscopy [28]. Finally, the Rydberg laser with wavelength $\lambda_R = 790.3$ nm, Rabi frequency Ω_R, and waist $w_R = 80$ μm is tuned around the resonance between the excited state $7s_{1/2}$ and the Rydberg state $26p_{3/2}$.

For a multiphoton transition to a Rydberg state, the transmission of the probe light resonant with the optical transition is increased by population shelving in the Rydberg state [29] and provides a direct readout of the Rydberg population. The change in probe laser transmission ΔT as a function of Rydberg laser detuning Δ_R is shown in Fig. 2(c) for increasing the Rydberg Rabi frequency Ω_R. As the level of Rydberg population increases, the excitation-dependent shift first produces an asymmetry in the line shape (ii). Eventually, when the shift is greater than the linewidth (iii), the line shape exhibits intrinsic
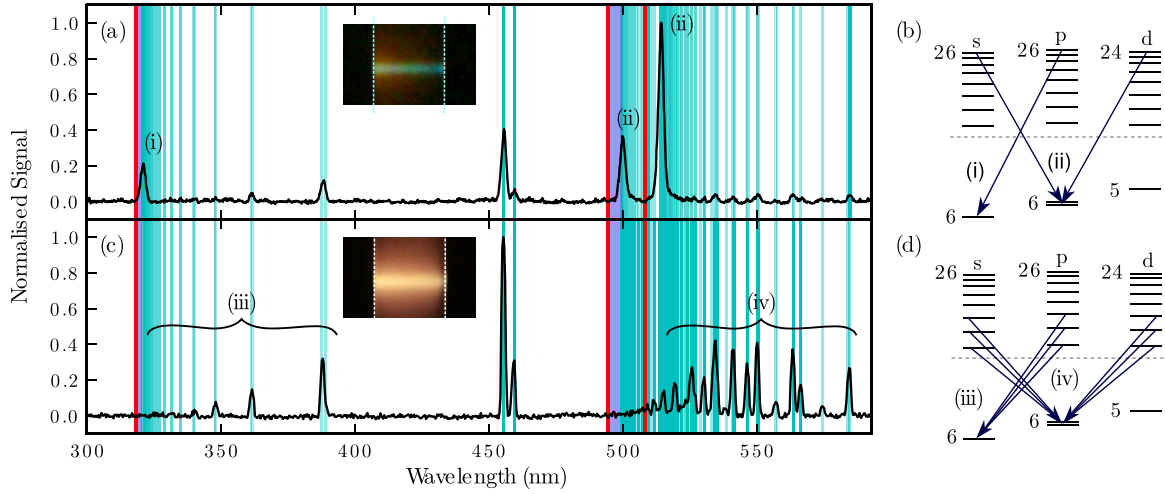
FIG. 3 (color online).   Atomic emission spectra for low and high Rydberg state occupancy. The visible fluorescence spectrum is shown for (a) $\mathcal{N} = 3.1 \times 10^{11}$ cm^{-3} and (c) $\mathcal{N} = 4.3 \times 10^{12}$ cm^{-3}. In the low Rydberg occupancy phase, the spontaneous emission originates from high-lying Rydberg states as illustrated in (b). However, in the high Rydberg occupancy phase, the spontaneous emission originates from low-lying Rydberg states, as illustrated in (d), due to a superradiant cascade between high-lying Rydberg states. The ionization limits from $6s_{1/2}$, $6p_{1/2}$, and $6p_{3/2}$ are shown by thick red vertical lines. The blue shaded regions highlight the absence of spontaneous emission between $26p_{3/2}$ and ionization which would occur due to a blackbody or collisional excitation process. The thin cyan vertical lines indicate the dipole-allowed transitions. Probe Rabi frequency $\Omega_{\mathrm{p}} = 2\pi \times 41$ MHz, coupling Rabi frequency $\Omega_{\mathrm{c}} = 2\pi \times 74$ MHz, and Rydberg Rabi frequency $\Omega_{\mathrm{R}} = 2\pi \times 122$ MHz.

optical bistability with hysteresis dependent on the direction in which resonance is approached (shown by the arrows). Importantly, this bistability is measured in steady state and is not a transient phenomenon. As a result, within the hysteresis window, the system can be placed in either the low or high Rydberg occupancy phase with exactly the same experimental parameters.

The change in atomic behavior across the phase transition can be analyzed by measuring the spectrum of the off-axis fluorescence. The emission spectra for the two phases of low and high occupancy are shown in Figs. 3(a) and 3(c), respectively. In the low phase, the dominant transitions indicated by (i) and (ii) involve decay from high-lying Rydberg states to the ground states of the s, p, and d series. This behavior highlighted in Fig. 3(b) is consistent with spontaneous emission where such transitions dominate due to the ω^3 dependence in the Einstein A coefficient. This phase is characterized by the faint (green) fluorescence shown in the inset.

In the high Rydberg occupancy phase, the emission spectrum is dramatically modified. The dominant spontaneous emission transitions (i) and (ii) are no longer present. Instead, the spontaneous emission now originates from a range of low-lying Rydberg states indicated by (iii) and (iv) and highlighted in Fig. 3(d). This phase is characterized by the strong (orange) fluorescence shown in the inset. Importantly, the absence of emission close to the ionization limit for each series indicated by the dark (red) vertical lines indicates that atoms are not promoted to higher-lying Rydberg states, as would occur in collisional or up-conversion processes [7]. We can also neglect the

effects of thermal blackbody photons because the average number of photons per mode at Rydberg-Rydberg transition frequencies is much lower than the average number of excited atoms [30]. The transitions at 455 and 459 nm occur in both phases and correspond to decay to $6s_{1/2}$ from $7p_{3/2}$ and $7p_{1/2}$, respectively.

The emission spectrum in the high occupancy phase can be understood as a superradiant cascade to lower-lying Rydberg states [31]. Evidence for a superradiant cascade has also been observed in ultracold atoms [32,33]. When the cooperativity on a particular transition is high, the atoms emit collectively and in phase with one another. The single atom lifetime of the $26p_{3/2}$ to $26s_{1/2}$ transition is $\tau \simeq 500$ μs but within the transition wavelength volume $V = 1$ mm^3, we estimate the Rydberg atom number $N_{\mathrm{R}} \simeq 5 \times 10^6$. Consequently, we expect a superradiant decay time scale of $\tau_{\mathrm{super}} = \tau/N_{\mathrm{R}} \simeq 100$ ps. As the transition wavelength and therefore the cooperative enhancement of the decay rate is proportional to n^3, the superradiant cascade eventually stops and gives rise to the observed spontaneous emission from low-lying Rydberg states as indicated by (iii) and (iv) in Fig. 3(c).

By stabilizing the laser frequency within the hysteresis window and varying the intensity of the Rydberg laser I_{R}, it is possible to observe bistability and hysteresis in the optical response as shown in Fig. 4(a). The system switches between the low occupancy phase with probe transmission level T_1 and the high occupancy phase with probe transmission level T_2. In this case, the phase transition from low to high Rydberg population occurs at critical intensity $I_{\mathrm{R,crit}} \approx 17.5$ W/mm^2.
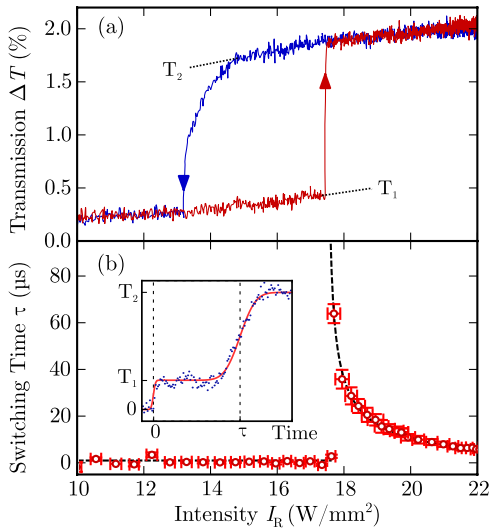
FIG. 4 (color online). Critical slowing down as the temporal signature of a phase transition. (a) Continuous Rydberg laser intensity I_R scan showing bistability and hysteresis in the optical response ΔT. (b) Discrete Rydberg laser intensity I_R scan showing the divergence of the switching time to steady-state τ around the critical transition intensity $I_{R,crit} \approx 17.5$ W/mm^2. The switching time diverges as $(I_R - I_{R,crit})^\alpha$ with critical exponent $\alpha = -0.53 \pm 0.10$ (standard deviation error) shown by the dashed line of best fit. Ground-state density $\mathcal{N} = 4.3 \times 10^{12}$ cm^{-3}, probe Rabi frequency $\Omega_p = 2\pi \times 57$ MHz, coupling Rabi frequency $\Omega_c = 2\pi \times 116$ MHz, and Rydberg detuning $\Delta_R = 2\pi \times -220$ MHz. The error bars represent the standard deviation error on the determination of the laser intensity and switching time.

The first-order phase transition between the low and high Rydberg occupancy phases can be confirmed through the observation of critical slowing down. This temporal signature of a phase transition occurs as the system approaches a critical point and becomes increasingly slow at recovering from perturbations [34,35]. The temporal response of the ensemble is measured by discretely varying the Rydberg laser intensity I_R and measuring the time τ to reach steady state, as illustrated in the inset of Fig. 4(b). At the critical transition, the switching time diverges according to the power law $\tau \propto (I_R - I_{R,crit})^\alpha$ shown by the fitted dashed line. The critical exponent $\alpha = -0.53 \pm 0.10$ (standard deviation error) is consistent with previous work on first-order phase transitions and optical bistability [36,37].

We also note that the geometry of the excitation region plays an important role in our observation of many-body dynamics [38]. The optical path length of 2 mm provided by the vapor cell is comparable to the interaction wavelength. If the medium was much shorter, the cooperative shift would not result in intrinsic optical bistability. Furthermore, if the medium was much longer, the dipoles would not evolve with the same phase. A more complete study of the length dependence of the effect will form the focus of future work.

In summary, we have demonstrated a cooperative nonequilibrium phase transition in a dilute thermal atomic gas. The observations that have been discussed raise interesting possibilities for future nonlocal propagation experiments which utilize the long-range cooperative interaction [18]. Furthermore, this work could be used to perform precision sensing [39] around the critical point and to study resonant energy transfer [40] on optically resolvable length scales. In addition, studies of the fluorescence in the vicinity of the phase transition could provide further insight into the dynamics of strongly interacting dissipative quantum systems [20,21].

[1] H. Haken, Naturwissenschaften **67**, 121 (1980).
[2] H. M. Gibbs, S. L. McCall, and T. N. C. Venkatesan, Phys. Rev. Lett. **36**, 1135 (1976).
[3] H. M. Gibbs, *Optical Bistability: Controlling Light with Light* (Academic Press, New York, 1985).
[4] H. J. Carmichael and D. F. Walls, J. Phys. B **10**, L685 (1977).
[5] D. F. Walls, P. D. Drummond, S. S. Hassain, and H. J. Carmicheal, Prog. Theor. Phys. Suppl. **64**, 307 (1978).
[6] C. M. Bowden and C. C. Sung, Phys. Rev. A **19**, 2392 (1979).
[7] M. P. Hehlen, H. U. Güdel, Q. Shu, J. Rai, S. Rai, and S. C. Rand, Phys. Rev. Lett. **73**, 1103 (1994).
[8] J. Keaveney, A. Sargsyan, U. Krohn, I. G. Hughes, D. Sarkisyan, and C. S. Adams, Phys. Rev. Lett. **108**, 173601 (2012).
[9] F. A. Hopf, C. M. Bowden, and W. H. Louisell, Phys. Rev. A **29**, 2591 (1984).
[10] R. Friedberg, S. R. Hartmann, and J. T. Manassah, Phys. Rev. A **39**, 3444 (1989).
[11] M. D. Lukin, M. Fleischhauer, R. Cote, L. M. Duan, D. Jaksch, J. I. Cirac, and P. Zoller, Phys. Rev. Lett. **87**, 037901 (2001).
[12] M. Saffman, T. G. Walker, and K. Mølmer, Rev. Mod. Phys. **82**, 2313 (2010).
[13] J. D. Pritchard, K. J. Weatherill, and C. S. Adams, *Annual Review of Cold Atoms and Molecules* (World Scientific, Singapore, 2013).
[14] Y. O. Dudin and A. Kuzmich, Science **336**, 887 (2012).
[15] T. Peyronel, O. Firstenberg, Q.-Y. Liang, S. Hofferberth, A. V. Gorshkov, T. Pohl, M. D. Lukin, and V. Vuletić, Nature (London) **488**, 57 (2012).
[16] D. Maxwell, D. J. Szwer, D. Paredes-Barato, H. Busche, J. D. Pritchard, A. Gauguet, K. J. Weatherill, M. P. A. Jones, and C. S. Adams, Phys. Rev. Lett. **110**, 103001 (2013).

[17] P. Schauss, M. Cheneau, M. Endres, T. Fukuhara, S. Hild, A. Omran, T. Pohl, C. Gross, S. Kuhr, and I. Bloch, Nature (London) **491**, 87 (2012).

[18] S. Sevinçli, N. Henkel, C. Ates, and T. Pohl, Phys. Rev. Lett. **107**, 153001 (2011).

[19] T. E. Lee, H. Häffner, and M. C. Cross, Phys. Rev. A **84**, 031402 (2011).

[20] T. E. Lee, H. Häffner, and M. C. Cross, Phys. Rev. Lett. **108**, 023602 (2012).

[21] C. Ates, B. Olmos, J. P. Garrahan, and I. Lesanovsky, Phys. Rev. A **85**, 043620 (2012).

[22] T. Baluktsian, B. Huber, R. Löw, and T. Pfau, Phys. Rev. Lett. **110**, 123001 (2013).

[23] R. Friedberg, S. R. Hartmann, and J. T. Manassah, Phys. Rep. **7**, 101 (1973).

[24] See Supplemental Material at http://link.aps.org/supplemental/10.1103/PhysRevLett.111.113901 for the solution of Eq. (1).

[25] C. Carr, M. Tanasittikosol, A. Sargsyan, D. Sarkisyan, C. S. Adams, and K. J. Weatherill, Opt. Lett. **37**, 3858 (2012).

[26] M. Tanasittikosol, C. Carr, C. S. Adams, and K. J. Weatherill, Phys. Rev. A **85**, 033830 (2012).

[27] See Supplemental Material at http://link.aps.org/supplemental/10.1103/PhysRevLett.111.113901 for details of the four-level optical Bloch model.

[28] C. Carr, C. S. Adams, and K. J. Weatherill, Opt. Lett. **37**, 118 (2012).

[29] P. Thoumany, T. Germann, T. Hänsch, G. Stania, and L. Urbonas, Th. Becker, J. Mod. Opt. **56**, 2055 (2009).

[30] J. M. Raimond, P. Goy, M. Gross, C. Fabre, and S. Haroche, Phys. Rev. Lett. **49**, 1924 (1982).

[31] F. Gounand, M. Hugon, P. R. Fournier, and J. Berlande, J. Phys. B **12**, 547 (1979).

[32] T. Wang, S. F. Yelin, R. Côté, E. E. Eyler, S. M. Farooqi, P. L. Gould, M. Koštrun, D. Tong, and D. Vrinceanu, Phys. Rev. A **75**, 033802 (2007).

[33] K. J. Weatherill, J. D. Pritchard, R. P. Abel, M. G. Bason, A. K. Mohapatra, and C. S. Adams, J. Phys. B **41**, 201002 (2008).

[34] R. Bonifacio and P. Meystre, Opt. Commun. **29**, 131 (1979).

[35] M. Scheffer, J. Bascompte, W. A. Brock, V. Brovkin, S. R. Carpenter, V. Dakos, H. Held, E. H. van Nes, M. Rietkerk, and G. Sugihara, Nature (London) **461**, 53 (2009).

[36] G. Grynberg and S. Cribier, J. Phys. (Paris), Lett. **44**, 449 (1983).

[37] P. C. Hohenberg and B. I. Halperin, Rev. Mod. Phys. **49**, 435 (1977).

[38] R. Friedberg and J. T. Manassah, Phys. Rev. A **84**, 023839 (2011).

[39] R. P. Abel, C. Carr, U. Krohn, and C. S. Adams, Phys. Rev. A **84**, 023408 (2011).

[40] M. Sarovar, A. Ishizaki, G. R. Fleming, and K. B. Whalley, Nat. Phys. **6**, 462 (2010).